First-order transition in the weak ferromagnetic state of $ErNi_2{}^{11}B_2C$

H. Kawano-Furukawa and Y. Ishida
Graduate School of Humanities and Sciences, Ochanomizu University, Tokyo 112-8610, Japan

T. Nagata
Department of Physics, Ochanomizu University, Tokyo 112-8610, Japan

S. Ohira-Kawamura and C. Kobayashi
Academic and Information Board, Ochanomizu University, Bunkyo-ku, Tokyo 112-8610, Japan

H. Yoshizawa
Neutron Science Laboratory, Institute for Solid State Physics, The University of Tokyo, Ibaraki 319-1106, Japan

H. Takeya
National Institute for Materials Science, Tsukuba, Ibaraki 305-0047, Japan
(Received 4 May 2008; published 13 August 2008)

A detailed investigation of the ordering process of a weak ferromagnetic state in superconducting $ErNi_2{}^{11}B_2C$ was made by a neutron-diffraction technique. The results reveal that there are at least two magnetic phase transitions around ~2.3 K related to a weak ferromagnetic ordering process. We conclude that one of the two transitions is of the first order and corresponds to a rotation of spins from the *a* to the *b* axis. Details of the spin arrangements in a weak ferromagnetic state were also reconsidered. The data reveal that clear magnetic peaks appear at $\boldsymbol{Q}$ positions with $\boldsymbol{q}=(1\ 0\ 0)$ in the weak ferromagnetic state, which are prohibited by extinction rules in the model proposed by Jensen [Phys. Rev. B **65**, 140514 (2002)].

DOI: 10.1103/PhysRevB.78.064411 PACS number(s): 74.25.Ha, 75.30.Fv, 74.70.Dd, 75.25.+z

I. INTRODUCTION

Since the discovery of new quaternary intermetallic borocarbide superconductors, RT_2B_2C ($R=Y$ and rare earth and $T=$transition metal),[1–3] coexistence states between magnetism and superconductivity (SC) have been extensively revisited.[4,5] The highest T_c of this family is 23 K for YPd_2B_2C and coexisting states between magnetic orders and SC were observed in several systems with magnetic rare-earth (R) atoms, e.g., Tm, Ho, Er, Dy, etc. and $T=$Ni and Pt. The main magnetic interaction in these systems is the Ruderman-Kittel-Kasuya-Yosida type between the conduction electrons on T sites and localized ones on R atoms.[6] This interaction is mainly caused by Fermi-surface nesting that is strong enough to cause clear Kohn anomalies in phonon-dispersion curves.[7–9] The crystal structure of RT_2B_2C consists of alternative stacking between R-C and Ni_2-B_2 layers along the c axis and the R atoms occupy body-centered positions.[10] Among the family, $ErNi_2B_2C$ is the only system in which a *microscopic* and *stable* coexisting state between weak ferromagnetism (WFM) and SC was confirmed.[11–14]

$ErNi_2B_2C$ first transforms to the SC state below $T_c=10.5$ K. At lower temperature, it enters the Néel state below $T_N\sim 6$ K. At an early stage of studies on this compound, Zarestky *et al.*[15] and Sinha *et al.*[16] independently performed neutron-diffraction measurements. Both groups observed that clear magnetic peaks develop below T_N at $\boldsymbol{Q}$ positions with an incommensurate propagation vector $\boldsymbol{q}\sim 0.553\boldsymbol{a}^*$, and confirmed that the spins on the Er atoms form a transversely polarized planar sinusoidal structure (spins $\|\boldsymbol{b}$ and $\boldsymbol{q}\|\boldsymbol{a}^*$). They also confirmed that such a spin-density wave (SDW) structure squares up at a lower temperature by observing the developments of odd-number higher-order peaks at the $3\boldsymbol{q}$ and $5\boldsymbol{q}$ positions.

After these works, in 1996, Canfield *et al.*[11] reported that a small cusp appears at $T_{WFM}\sim 2.3$ K in temperature dependence of the specific heat and by combining the results of the magnetization measurements they proposed the existence of the WFM order in $ErNi_2B_2C$. In order to check this exotic possibility, we performed unpolarized and half-polarized neutron-diffraction measurements[12,13] and then succeeded to confirm the appearance of an interference term, the difference between nonspin flip I_{++} and I_{--} intensities, in half-polarized experiments at both (0 0 2) and (0 0 6) nuclear Bragg positions below T_{WFM}. This provides direct evidence for *microscopic* coexistence between the WFM and the SC in $ErNi_2B_2C$.[13]

In those studies, we further confirmed that in the WFM phase the propagation vector of the SDW order locks into a commensurate value of $0.55\boldsymbol{a}^*$ ($=11/20\boldsymbol{a}^*$) and that there appear higher-order peaks of this propagation vector at $(n/20\ 0\ 0)$ with not only $n=$odd but also $n=$even. The appearance of higher-order peaks at $(n/20\ 0\ 0)$ with $n=$odd was attributed to a squaring up of the SDW order, as before, but peaks with $n=$even (which can be written as $(m/10\ 0\ 0)$ positions with $m=$integer) required other reasons.

In a previous paper,[17] we proposed a model for the WFM phase in which the appearance of higher-order peaks with $n=$even was attributed to the WFM order for the following reasons. In the WFM phase with a commensurate propagation vector of $q=0.55\boldsymbol{a}^*$, the magnetic unit cell becomes $20a\times b\times c$, which contains 40 Er atoms. There can appear two nodal positions on sites and they form a unit cell with dimensions of $10a\times b\times c$. At such nodal positions (because

no internal field affects the spin directions) one can assume any spin configurations among them. When we put ferromagnetic moments on these nodal positions [see Fig. 4(c)], the model could not only reproduce the appearance of magnetic Bragg peaks at every $(m/10\ 0\ 0)$ position with m =integer but also gives rise to a WFM net moment of 0.39 μ_B/Er, which is reasonably close to the observed value (=0.35 μ_B/Er at 1.8 K) based on magnetization measurements.

Choi *et al.*[14] performed similar neutron-diffraction measurements and reported very similar scattering patterns. In addition, Jensen[18] performed mean-field calculations and then proposed a different model for the spin arrangement in the WFM phase. His model can be obtained by flipping one down spin up in our model [Fig. 4(d)], and four spins among the 40 Er ones contributed to the WFM. Although their model gives rise to a double-size net moment of 0.78 μ_B/Er, it can reproduce the neutron-diffraction pattern with the same level as our model.

The discrepancy in the two models for the spin arrangement in the WFM phase has required more detailed experiments. Furthermore, the origin of the WFM and its ordering process are still unclear. Especially, we have noticed that the temperature-dependence data of our previous neutron-diffraction measurements always show a clear hysteresis around $T \sim T_{\mathrm{WFM}}$, indicating the possibility of a contribution of a first-order-type transition. This is in sharp contrast with the previously proposed second-order scenario based on the anomaly observed in specific-heat measurements.[11] In order to resolve these uncertainties in the nature of the WFM phase in $ErNi_2B_2C$, we performed a second series of neutron-diffraction measurements.

In the present work, we confirm that the system possesses at least two phase transitions around $T_{\mathrm{WFM}} \sim 2.3$ K and that one of the transitions can be attributed to a rotation of spins within the easy ab plane, and that it is of the first order. Furthermore, we provide different aspects to lead readers to duly appreciate differences in the two models for the spin arrangements in the WFM phase and then a resultant demand to solve the problem. The present results show that our model satisfies such a demand.

II. EXPERIMENTAL PROCEDURE

Single crystals of $ErNi_2{}^{11}B_2C$ were grown by the floating zone method. The details of the growth technique were previously reported.[19] T_c of our sample was determined to be $\sim$8.6 K by a magnetization measurement, which is a rather low value for the $ErNi_2B_2C$ system. With another piece from the same crystal, annealing raised the T_c but did not cause any detectable change in the magnetic properties. This result indicates that microscopic defects in as-grown samples lower T_c. In the present study, we used an unannealed sample with $T_c \sim 8.6$ K, which was the same crystal as that used in our previous experiment.[12,13,17]

Unpolarized neutron-diffraction experiments were performed using the triple-axis spectrometers, GPTAS (4G) and HER (C1–1), installed at the JRR-3 research reactor and its guide hall at the Japan Atomic Energy Agency in Tokai (Japan). Neutrons with momenta of k_f=2.67 and 1.55 Å^{-1} were selected by (0 0 2) reflection of pyrolytic graphite (PG) monocrometers. The spectrometers were set in elastic two-axis (4G) and triple-axis (C1–1) modes and combinations of collimators, 40′-40′-40′ (4G) and open-open-40′-80′ (C1–1) before the monochromator to the detector, were utilized. PG (4G) and Be(C1–1) filters were placed before the sample positions to eliminate any higher-order contamination.

A single crystal with dimensions of $\sim 5mm\phi \times 10$ mm was set in an aluminum can, in such a way, to study the $(h\ 0\ l)$ scattering plane. The can was filled with He exchange gas to ensure a uniform temperature. A 1 K cryostat (^{3}He-^{4}He gas cycling system type) and an orange cryostat (liquid He type) were used. The lowest temperature of the measurements was $\sim$0.7 K with a 1 K cryostat. The lattice parameters at room temperature with tetragonal symmetry were $a=b=3.5014$ Å and $c=10.530$ Å.

Note that it is known that the crystal symmetry of RNi_2B_2C is lowered from tetragonal ($I4/mmm$) to orthorhombic ($Immm$) when the system enters the SDW state due to a strong spin-orbit coupling.[20] The temperature dependence of the lattice parameters has already been taken into account in all of the results discussed in the present paper.

III. RESULTS AND DISCUSSIONS

A. Ordering process to the WFM state

Depicted in Fig. 1(a) is the temperature dependence of the integrated intensity observed at a fundamental SDW peak position with $\boldsymbol{Q}=\boldsymbol{q} \sim (0.55\ 0\ 0)$. With decreasing temperature, the intensity first shows an abrupt increase around 6 K, indicating that the SDW order takes place at T_N. With further decreasing temperature, it exhibits a saturated behavior below 5 K but a second increase sets in below $\sim$2.3 K. The second increase can be attributed to the WFM transition because the temperature corresponds to T_{WFM}, although it does not require that the WFM order parameter itself contributes to the Bragg intensity at this $\boldsymbol{Q}$ position. The inset of Fig. 1(a) shows an enlarged figure of the low-temperature region. It appears that there is hysteresis. Namely, the onset temperature of the second increase with cooling is lower than in heating. This result indicates the contribution of a first-order-type transition to the WFM ordering process.

On the other hand, Fig. 1(b) shows the temperature dependence of the h position of the $3\boldsymbol{q}$ peak. A clear hysteresis behavior is observed in the two measuring processes. A clear bump appears around 2.3 K only in data taken during the cooling process. This anomaly at $T \sim T_{\mathrm{WFM}}$ was observed not only at the $3\boldsymbol{q}$ position but also at other higher-order positions such as $5\boldsymbol{q}$ and $7\boldsymbol{q}$. These results do not exclude the possibility of the first-order type transition in the WFM ordering process.

Note that the dotted line in Fig. 1(b) indicates an h position corresponding to the commensurate propagation vector of $\boldsymbol{q}=11/20\boldsymbol{a}^*$. The temperature dependence of the lattice parameter a was taken into account when we evaluated the h value for the $3\boldsymbol{q}$ peak. However, the data clearly show systematic shifts from the commensurate value. This can be

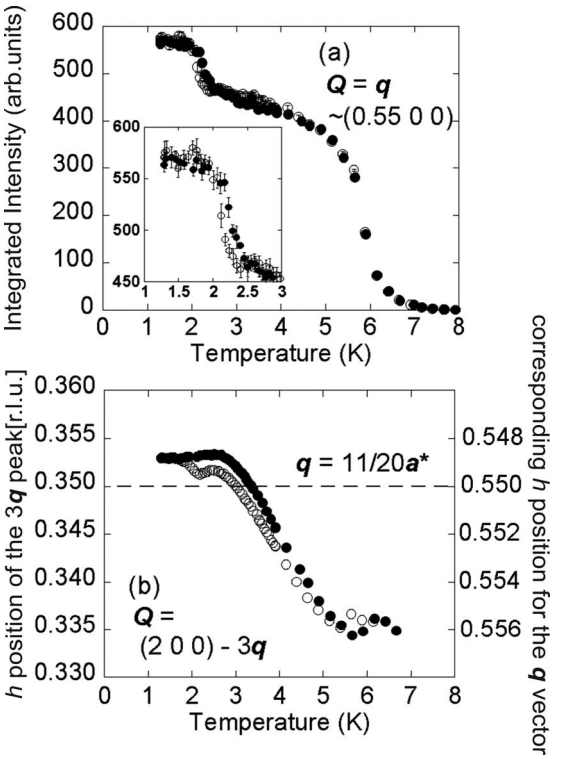

FIG. 1. (a) Temperature dependence of the integrated intensity of the fundamental SDW peak observed at $\boldsymbol{Q}=\boldsymbol{q}\sim(0.55\ 0\ 0)$. Inset: an enlargement of the low-temperature part of (a). (b) Temperature dependence of the h position for the $3\boldsymbol{q}$ peak observed at (2 0 0)-$3\boldsymbol{q}$. The right side vertical axis denotes the corresponding $\boldsymbol{q}$ position. The open and closed symbols indicate data taken in cooling and heating processes, respectively.

attributed to limitations of angular controls in diffraction measurements ($\sim$0.01°). We determined the h value of the propagation vector $\boldsymbol{q}$ from the h position of the $19\boldsymbol{q}$ peak, which gives the highest accuracy compared to other higher-order peak positions.

In order to see changes in the WFM order parameter in detail, we measured the temperature dependence of the Bragg intensities at $\boldsymbol{Q}$ positions of (1 0 0), (0 0 1), (2 0 0), and (0 0 2). The results are depicted in Figs. 2; (1 0 0) and (0 0 1) are the $\boldsymbol{Q}$ positions where only the WFM order parameter contributes to the scattering intensity, but the latter two $\boldsymbol{Q}$ positions (2 0 0) and (0 0 2) are concurrent with nuclear Bragg points.

As shown in Figs. 2(c) and 2(d), the intensities at (2 0 0) and (0 0 2) show abrupt increases below T_N, which can be attributed to changes in the nuclear structure factors due to a strong spin-orbit coupling. However, no clear changes are observed at T_{WFM}. This result can be interpreted that the nuclear structure factors at these two Bragg points are large and the magnetic contributions below T_{WFM} are overwhelmed. On the other hand, the intensities at (1 0 0) and (0 0 1) do not show any changes at T_N but abrupt increases below T_{WFM}, although they show a different temperature dependence. Namely, the intensity at (0 0 1) shows a gradual increase below $T_{\mathrm{WFM}}=2.3$ K and a clear jump at around $T_{\mathrm{R}}\sim 1.8$ K but at (1 0 0) only a sudden increase appears at

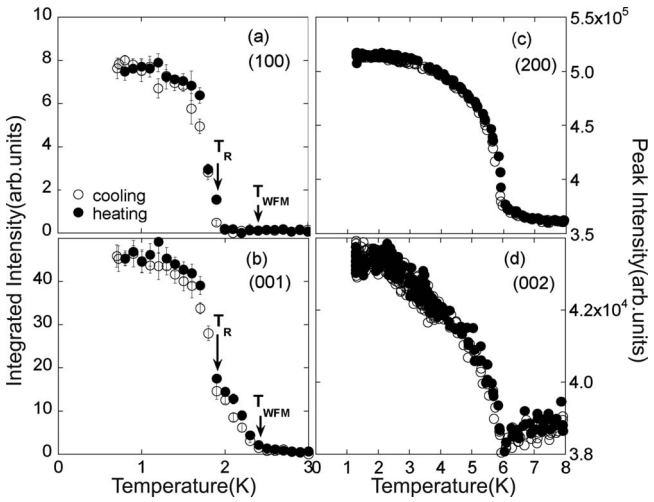

FIG. 2. Temperature dependence of the neutron-diffraction intensity at the WFM Bragg positions (a) (1 0 0), (b) (0 0 1), (c) (2 0 0), and (d) (0 0 2). The latter two also correspond to the nuclear Bragg positions for $ErNi_2B_2C$ with a body-centered orthorhombic crystal structure (space-group *Immm*).

T_{R}. This discrepancy in their temperature dependences can be interpreted by the orientation factor. That is to say, the ordering process of the moments on the *bc* plane can be observed at Bragg points (1 0 0) but that on the *ab* plane at (0 0 1). From this fact, one can interpret that the WFM order first develops with the moments along the *a* axis below $T_{\mathrm{WFM}}=2.3$ K, but that the easy axis of this order suddenly changes to the *b* axis at T_{R}. From the sudden change at T_{R} and the hysteresis behavior observed in the temperature-dependence data, we concluded that the phase transition at T_{R} is of the first order. Hereafter, we call the phase between $T_{\mathrm{R}}\leq T\leq T_{\mathrm{WFM}}$ the WFM phase (I) and that below T_{R} the WFM phase (II).

In order to further understand the ordering process to the WFM phases (I) and (II), we measured magnetic profiles along (h 0 0) and (h 0 1) at selected temperatures. Shown in Figs. 3(a)–3(d) are portions of the magnetic profiles observed along (h 0 0) at 3.0 K (SDW phase) in Fig. 3(a), 1.9 K [WFM phase (I)] in Fig. 3(b), and 0.7 K [WFM phase (II)] in Fig. 3(c) and that along (h 0 1) at 2.2 K [WFM phase (I)] in Fig. 3(d). The bottom axis for Fig. 3(d) is reversed to show the same q region as in Figs. 3(a)–3(c).

At 3 K in the SDW phase [Fig. 3(a)], $\boldsymbol{q}$ and its higher-order peaks are observed. Among the higher-order peaks, the $2\boldsymbol{q}$ peaks observed at (0.9 0 0) and (1.1 0 0) are attributed to lattice distortions along the *a* axis due to strong spin-orbit coupling. Furthermore, the existence of odd-number higher-order peaks reveals that the SDW order tends to square up. On the other hand, at 0.7 K in the WFM phase (II) [Fig. 3(c)], there appear many magnetic peaks at (n/20 0 0) not only with n=odd but also n=even. As described in Sec. I, these higher-order peaks with n=even are attributed to the WFM order.[17] The WFM moments form a unit cell with dimensions of $10a\times b\times c$. These results are consistent with our previous results. This will be reconsidered in Sec. III B

At 1.9 and 2.2 K in the WFM phase (I), which was found in the present study, [Figs. 3(b) and 3(d)], in contrast to the

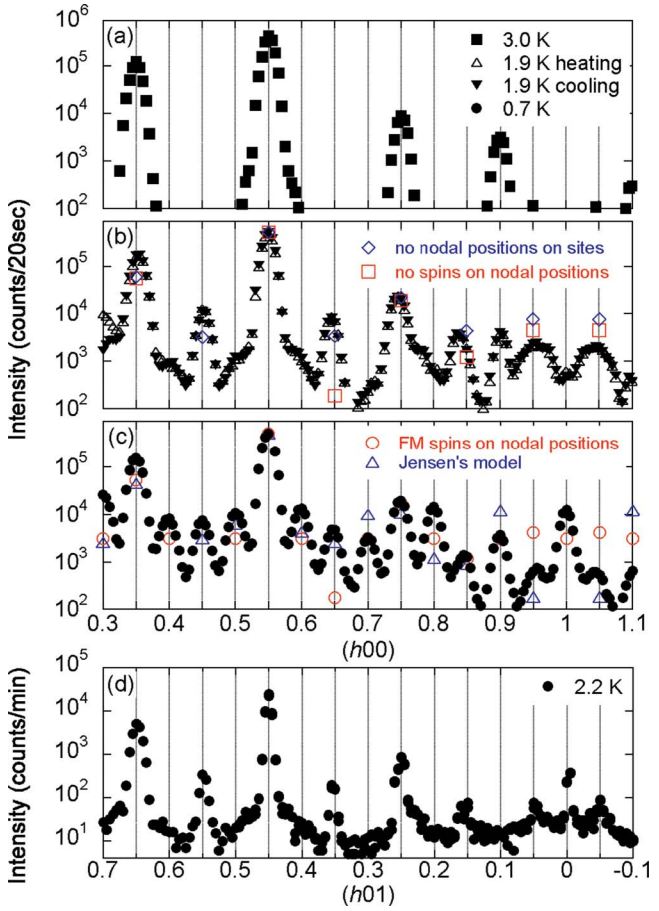

FIG. 3. (Color online) Magnetic profiles along (h 0 0) at (a) 3.0, (b) 1.9, and (c) 0.7 K, respectively, and along (h 0 1) at (d) 2.2 K. The background data taken at 10 K were already subtracted. The bottom axis for (d) is reversed so as to demonstrate the same $\boldsymbol{q}$ region with the figures shown above. The filled and open symbols denote data recorded in cooling and heating processes, respectively. The open symbols at every (n/20 0 0) positions with n=integer in (b) and (c) are the calculated intensities for the models shown in Fig. 4. Detailed explanations are given in the text.

WFM phase (II) and except for the $2\boldsymbol{q}$ peaks at (0.9 0 0) and (1.1 0 0) due to lattice distortion, an even-number higher-order magnetic Bragg peak is observed only at $\boldsymbol{Q}$=(0 0 1) and diffuse peaks at all other n=even positions. As described in Sec. I, our previous half-polarized neutron-diffraction measurements revealed that the interference terms of the neutron-diffraction method appear at (0 0 2) and (0 0 6) below 2.3 K, indicating that the WFM order of this compound takes place below this temperature. These facts indicate that the WFM first develops in such a way as to give nonzero magnetic structure factors at both $\boldsymbol{q}$=(0 0 0) and (1 0 0) positions but not at the other $\boldsymbol{q}$=(n/20 0 0) positions with n=even. This clearly requires that the WFM order develops among spins not only at nodal positions, which may appear at every $10a\times b\times c$ position with a commensurate propagation vector of $11/20\boldsymbol{a}^*$, but also those at all other positions. Furthermore, the fact that the peak with $\boldsymbol{q}$ =(1 0 0) is observed only at $\boldsymbol{Q}$=(0 0 1), but not at (1 0 0), requires that the WFM order develops with moments parallel to the a axis as discussed above. The present results reveal that the squared up SDW moments start to rotate toward the a axis below 2.3 K, developing the WFM order, but such a WFM order is suddenly broken off by developing the WFM order parallel to the b axis among the moments at the nodal positions below 1.8 K.

It should be noted here that $TbNi_2B_2C$ is another material that shows a similar SDW and WFM mixed order among the other RT_2B_2C systems, although it does not show a superconducting transition down to 300 mK.[21] Previous neutron-diffraction measurements confirmed that $TbNi_2B_2C$ shows the *longitudinal* SDW order below T_N=15 K with the moments parallel to the $\boldsymbol{a}$ axis and a propagation vector $\boldsymbol{q}$ $\sim 6/11\boldsymbol{a}^*$. Our recent neutron-diffraction results further revealed that the magnetic orders of this system consist of two independent SDW.[22] The $\boldsymbol{q}$ vectors of those SDW orders move with temperature but lock in at $\sim 11/20\boldsymbol{a}^* \pm 0.002\boldsymbol{b}^*$ and $6/11\boldsymbol{a}^*$ at low temperatures and the WFM order is found in the SDW with the latter $\boldsymbol{q}$.

The present results reveal that the WFM order in $ErNi_2B_2C$ first develops with magnetic moments that are parallel to the propagation vector as in $TbNi_2B_2C$. This fact indicates that the WFM ordering process in $TbNi_2B_2C$ should be referred to the $ErNi_2B_2C$ case, although the WFM order itself originates in different ways in the two materials. (The second SDW order with a different independent $\boldsymbol{q}$ wave appears to create the WFM order in the latter material.)

B. Spin arrangements in WFM phases (I) and (II)

In this section, we (re)consider the spin arrangements in the WFM phases (I) and (II). The magnetic unit cell in these phases is determined to be $20a\times b\times c$ by the size of the propagation vector of $11/20\boldsymbol{a}^*$. $ErNi_2B_2C$ has a body-centered structure so that the magnetic unit cell with $20a$ $\times b\times c$ contains 40 Er atoms; 20 Er atoms on the basal (z=0) planes and the 20 other atoms on the z=1/2 layers.

The magnetic neutron-diffraction intensities are associated with the Fourier transform of the spin components. Thus, one needs to determine the model which gives the best agreement with the observed diffraction patterns shown in Figs. 3(a)–3(d). As shown in Figs. 3(b) and 3(c) (in WFM phases) there appear clear higher-order peaks, indicating that the magnetic moments are rather squared up than forming a sinusoidal shape. Then, in order to make the analysis easier, we assume that all of spin components are parallel to the b axis and being fully up (S=1=↑), down (S=−1=↓), or zero (S=0).

Figures 4 show some models of the spin arrangements in the WFM phases (I) and (II). On the right-hand side, the spin arrangements on each (z=0 and 1/2) layer are depicted separately but on one layer in the left-hand side. The top panel [Fig. 4(a)] shows the spin arrangement with $\boldsymbol{q}=11/20\boldsymbol{a}^*$ without nodal positions on sites where all spins are up (S=1=↑) or down (S=−1=↓). This model is the same with theoretically proposed one for the SDW phase.[23] On the other hand, with a commensurate propagation vector, the system can have nodal positions on sites. Then, the second top panel shows such a model without any spins at the nodal

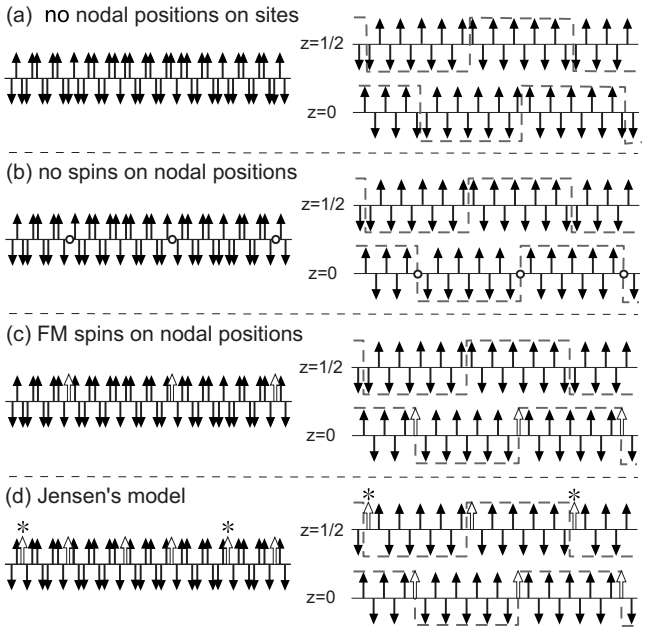

FIG. 4. Models of the magnetic structures in the WFM phases (I) and (II). On the right-hand side, the spin arrangements on each ($z=0$ and 1/2) layer are depicted separately but on one layer in the left-hand side. (a) No nodal positions on sites. (b) No spins on the nodal positions. (c) FM spins on the nodal positions. (d) Jensen's model, in which one down spin in the $z=1/2$ layer of the model (c) flips up. The positions of the spin are labeled with a "*" symbol. In each figure, the white arrows indicate the spins, which contribute to the WFM order of this material. For details, see the text.

positions. No net moments are produced with these two models. Figure 3(c) shows a model with $(\uparrow,\uparrow)$ spins at the nodal positions where two magnetic moments among 40 Er spins contribute to the ferromagnetic order, which gives rise to a net magnetic moment of $7.8\ \mu_B/\mathrm{Er}^*2/40=0.39\ \mu_B/\mathrm{Er}$, where $7.8\ \mu_B$ is the saturated moment per Er atom measured by magnetization curves. Finally, Fig. 4(d) shows a model proposed by Jensen[18] in which one down spin in the $z=1/2$ layer in our model [Fig. 4(c)] flips up. In this model, four magnetic moments among 40 Er spins contribute to the ferromagnetic order, which results in a double net moment of $7.8\ \mu_B/\mathrm{Er}^*4/40=0.78\ \mu_B/\mathrm{Er}$.

We calculated the magnetic neutron-diffraction intensities with these models; the results are shown in Figs. 3(b) and 3(c). As shown in Fig. 3(b) in WFM phase (I), the model shown in Fig. 4(a) can better reproduce the scattering pattern. This result is consistent with the idea that the WFM order develops among spins not only at nodal positions but also those at all other positions as discussed in Sec IIIA.

At first glance, it seems that the models shown in Figs. 4(c) and 4(d) can reproduce the scattering pattern at almost the same level in the WFM phase (II). From this point of view, one cannot judge which model gives a better agreement with the observed pattern. However, it should be pointed out here that the spin arrangements on the basal plane ($z=0$) and that on the $z=1/2$ layer are the same in Fig. 4(d), but not in Fig. 4(c), and that such a high symmetric spin arrangement in the former model leads to cancellations in the magnetic structure factors at very high-symmetry positions such as $\boldsymbol{q}=(1\ 0\ 0)$. The spin arrangement shown in Fig. 4(d) gives zero intensity at $\boldsymbol{q}=(1\ 0\ 0)$ and hence at $\boldsymbol{Q}=(1\ 0\ 0)$. However, there is a clear peak at $\boldsymbol{Q}=(1\ 0\ 0)$. This fact in turn indicates that the spin arrangement should be different between the $z=1/2$ and 0 layers. The model shown in Fig. 4(c) satisfies this condition and gives rise to the net moment of $0.39\ \mu_B/\mathrm{Er}$, which is closer to the observed value ($0.35\ \mu_B/\mathrm{Er}$ at 1.8 K) than that given by the model shown in Fig. 4(d). These facts let us conclude that the model shown in Fig. 4(c) is closer to the real spin arrangement in the WFM phase (II).

Finally, it should be mentioned that Walker and Detlefs[24] reported that the ferromagnetic order in RT_2B_2C should be accompanied by a lock-in transition of an SDW order to a commensurate propagation vector with $\boldsymbol{q}=(m/n)\boldsymbol{a}^*$ with m being even and n being odd. The WFM phases of $ErNi_2B_2C$ do not satisfy this condition. The reason for this discrepancy is still an open question.

IV. SUMMARY

Neutron-diffraction measurements were performed in order to investigate the ordering process and the detailed spin arrangement in the WFM state in superconducting $ErNi_2{}^{11}B_2C$. The results reveal that there are at least two magnetic phase transitions around ~2.3 K related to its WFM ordering processes and that one of them is of the first order. More detailed measurements reveal that this first-order transition corresponds to a rotation of spins from the a to the b axis. Furthermore, it appeared that the squared up SDW moments start to rotate toward the a axis below 2.3 K, developing the WFM order, but this WFM order is suddenly broken off by developing the WFM order parallel to the b axis among the moments at the nodal positions below 1.8 K. In addition, details of the spin arrangements in the WFM states were also reinvestigated. The data reveal that clear magnetic peaks appear at $\boldsymbol{q}=(1\ 0\ 0)$. We showed that this peak position is prohibited by extinction rules for the model proposed by Jensen.

[1] R. Nagarajan, C. Mazumdar, Z. Hossain, S. K. Dhar, K. V. Gopalakrishnan, L. C. Gupta, C. Godart, B. D. Padalia, and R. Vijayaraghavan, Phys. Rev. Lett. **72**, 274 (1994).

[2] R. J. Cava, H. Takagi, B. Batlogg, H. W. Zandbergen, J. J. Krajewski, W. F. Peck, Jr., R. B. van Dover, R. J. Felder, T. Siegrist, K. Mizuhashi, J. O. Lee, H. Eisaki, S. A. Carter, and S. Uchida, Nature (London) **367**, 146 (1994).

[3] R. J. Cava, H. Takagi, H. W. Zandbergen, J. J. Krajewski, W. F. Peck, Jr., T. Siegrist, B. Batlogg, R. B. van Dover, R. J. Felder, K. Mizuhashi, J. O. Lee, H. Eisaki, and S. Uchida, Nature (Lon-

don) **367**, 252 (1994).
[4] H. Eisaki, H. Takagi, R. J. Cava, B. Batlogg, J. J. Krajewski, W. F. Peck, Jr., K. Mizuhashi, J. O. Lee, and S. Uchida, Phys. Rev. B **50**, 647 (1994).
[5] J. W. Lynn, S. Skanthakumar, Q. Huang, S. K. Sinha, Z. Hossain, L. C. Gupta, R. Nagarajan, and C. Godart, Phys. Rev. B **55**, 6584 (1997).
[6] J. Y. Rhee, X. Wang, and B. N. Harmon, Phys. Rev. B **51**, 15585 (1995).
[7] P. Dervenagas, M. Bullock, J. Zarestky, P. Canfield, B. K. Cho, B. Harmon, A. I. Goldman, and C. Stassis, Phys. Rev. B **52**, R9839 (1995).
[8] H. Kawano, H. Yoshizawa, H. Takeya, and K. Kadowaki, Phys. Rev. Lett. **77**, 4628 (1996).
[9] H. Kawano, H. Yoshizawa, H. Takeya, and K. Kadowaki, Physica C **282-287**, 1055 (1997).
[10] T. Siegrist, H. W. Zandbergen, R. J. Cava, J. J. Krajewski, and W. F. Peck, Jr., Nature (London) **367**, 254 (1994).
[11] P. C. Canfield, S. L. Bud'ko, and B. K. Cho, Physica C **262**, 249 (1996).
[12] H. Kawano, H. Takeya, H. Yoshizawa, and K. Kadowaki, J. Phys. Chem. Solids **60**, 1053 (1999).
[13] H. Kawano-Furukawa *et al.*, in *Rare Earth Transition Metal Borocarbides (Nitrides): Superconducting, Magnetic and Normal State Properties*, NATO Advanced Studies Institute, Series II: Mathematics, Physics, and Chemistry Vol. 14, edited by K. H. Muller and V. Narozhnyi (Kluwer, Dordrecht, 2001), p. 223.
[14] S.-M. Choi, J. W. Lynn, D. Lopez, P. L. Gammel, P. C. Canfield, and S. L. Bud'ko, Phys. Rev. Lett. **87**, 107001 (2001).
[15] J. Zarestky, C. Stassis, A. I. Goldman, P. C. Canfield, P. Dervenagas, B. K. Cho, and D. C. Johnston, Phys. Rev. B **51**, 678 (1995).
[16] S. K. Sinha, J. W. Lynn, T. E. Grigereit, Z. Hossain, L. C. Gupta, R. Nagarajan, and C. Godart, Phys. Rev. B **51**, 681 (1995).
[17] H. Kawano-Furukawa, H. Takeshita, M. Ochiai, T. Nagata, H. Yoshizawa, N. Furukawa, H. Takeya and K. Kadowaki, Phys. Rev. B **65**, 180508(R) (2002).
[18] J. Jensen, Phys. Rev. B **65**, 140514(R) (2002).
[19] H. Takeya, T. Hirano, and K. Kadowaki, Physica C **256**, 220 (1996).
[20] C. Song, Z. Islam, L. Lottermoser, A. I. Goldman, P. C. Canfield, and C. Detlefs, Phys. Rev. B **60**, 6223 (1999).
[21] C. V. Tomy, L. A. Afalfiz, M. R. Lees, J. M. Martin, D. M. Paul, and D. T. Adroja, Phys. Rev. B **53**, 307 (1996).
[22] H. Kawano-Furukawa, H. Tsukagoshi, T. Nagata, C. Kobayashi, H. Yoshizawa, and H. Takeya, Phys. Rev. B **77**, 144426 (2008).
[23] A. Jensen, K. Nørgaard Toft, A. B. Abrahamsen, D. F. McMorrow, M. R. Eskildsen, N. H. Andersen, J. Jensen, P. Hedegård, J. Klenke, S. Danilkin, K. Prokes, V. Sikolenko, P. Smeibidl, S. L. Bud'ko and P. C. Canfield, Phys. Rev. B **69**, 104527 (2004).
[24] M. B. Walker and C. Detlefs, Phys. Rev. B **67**, 132407 (2003).